RESEARCH ARTICLE | APRIL 21 2023

A perspective on the doping of transition metal dichalcogenides for ultra-scaled transistors: Challenges and opportunities

Rehan Younas 💿 ; Guanyu Zhou 💿 ; Christopher L. Hinkle 🔀 💿

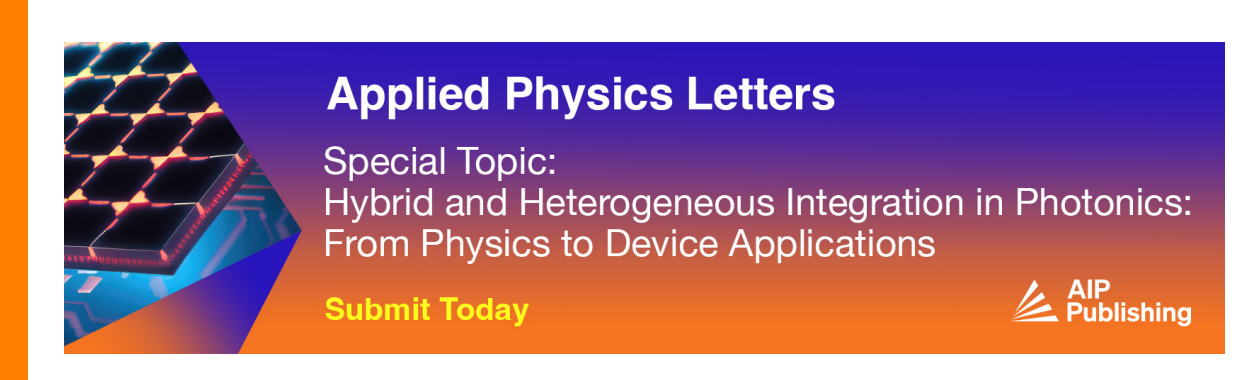


Appl. Phys. Lett. 122, 160504 (2023) https://doi.org/10.1063/5.0133064





CrossMark





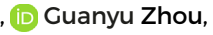
A perspective on the doping of transition metal dichalcogenides for ultra-scaled transistors: Challenges and opportunities (1) (3)

Cite as: Appl. Phys. Lett. 122, 160504 (2023); doi: 10.1063/5.0133064 Submitted: 1 November 2022 · Accepted: 17 March 2023 · Published Online: 21 April 2023









Rehan Younas, in Guanyu Zhou, in and Christopher L. Hinkle in



AFFILIATIONS

Department of Electrical Engineering, University of Notre Dame, Notre Dame, Indiana 46556, USA

a) Author to who correspondence should be addressed: chinkle@nd.edu

ABSTRACT

To support the ever-growing demand for faster, energy-efficient computation, more aggressive scaling of the transistor is required. Twodimensional (2D) transition metal dichalcogenides (TMDs), with their ultra-thin body, excellent electrostatic gate control, and absence of surface dangling bonds, allow for extreme scaling of the channel region without compromising the mobility. New device geometries, such as stacked nanosheets with multiple parallel channels for carrier flow, can facilitate higher drive currents to enable ultra-fast switches, and TMDs are an ideal candidate for that type of next generation front-end-of-line field effect transistor (FET). TMDs are also promising for monolithic 3D (M3D) integrated back-end-of-line FETs due to their ability to be grown at low temperature and with less regard to lattice matching through van der Waals (vdW) epitaxy. To achieve TMD FETs with superior performance, two important challenges must be addressed: (1) complementary n- and p-type FETs with small and reliable threshold voltages are required for the reduction of dynamic and static power consumption per logic operation, and (2) contact resistance must be reduced significantly. We present here the underlying strengths and weaknesses of the wide variety of methods under investigation to provide scalable, stable, and controllable doping. It is our Perspective that of all the available doping methods, substitutional doping offers the ultimate solution for TMDbased transistors.

Published under an exclusive license by AIP Publishing. https://doi.org/10.1063/5.0133064

I. INTRODUCTION

Two-dimensional transition metal dichalcogenides (TMDs) have gathered immense popularity for exhibiting exciting functionalities such as magnetism, ferroelectricity, and band structure modulation. The freedom to grow these materials on a variety of substrates without the strict condition of lattice matching underscores their potential for flexible electronics, heterostructures, and stacked chip architectures. Semiconducting TMDs, with their atomically thin bodies and desired bandgaps, show sufficient room temperature mobility and excellent gate electrostatic control.⁴ Their stability in the monolayer limit, immunity to short channel effects, and possible integration with industry compatible substrates make them promising candidates for both front-end-of-theline (FEOL) as well as back-end-of-the-line (BEOL) transistors. 5,6 To build complementary circuits based on TMDs and ensure consistent and reliable device performance over time, a number of issues still need to be addressed. These include improved large-area growth with digital thickness control and larger grains, scaled gate stacks with minimal interface traps, and air and water stability of the thin films.

One of the most important challenges associated with realizing high-performance TMD devices is the current lack of precise control over their carrier concentration, electrical conductivity, and threshold voltages. Additionally, the issue of high contact resistance (R_C) is arguably the biggest bottleneck in TMD-based nanoelectronics. To solve these issues, various doping methods such as electrostatic doping,^{7,8} conventional substitutional doping,^{9,10} intercalation,¹¹ and surface charge transfer doping ¹² are actively being researched along with newer methods such as reversible solid-state doping, 13 remote modulation doping, ¹⁴ and thickness modulation doping. ^{15,16} The rich choice of these doping techniques and the variety of TMDs available to the community render this area of research to be full of opportunities. At the same time, like any other nascent material system, there are several issues that must first be addressed.

Contrary to bulk materials with strong screening of Coulombic interactions, the reduced dimensionality of the 2D film causes a weak screening effect due to the change in the dielectric environment.¹⁷ This can be illustrated as shown in Fig. 1(a) in which the electric field

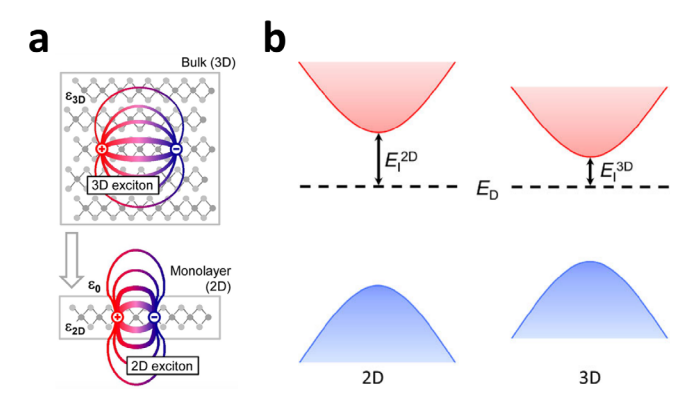


FIG. 1. (a) Schematic representation of the dielectric screening in a 3D vs 2D material. A different dielectric environment for the case of a 2D monolayer ($\varepsilon_{2D} > \varepsilon_o$) results in a weak screening of the Coulombic interaction. Reprinted with permission from Chernikov *et al.*, Phys. Rev. Lett. **113**, 076802 (2014). Copyright 2014 American Physical Society. (b) Schematic showing that the band edges move further away from the dopant state as the thickness of the semiconductor decrease due to the bandgap increase. Coupled with the weak screening, this results in a high ionization energy of the dopant. Reprinted with permission from Loh *et al.*, Nano Res. **14**, 1668–1681 (2021). Copyright 2021 Tsinghua University Press and Springer-Verlag GmbH Germany, part of Springer Nature.

lines joining an electron and hole extend outside of the 2D material into a low-k dielectric environment to weaken the screening effect. The screening experienced in 2D materials is quite different from the case for 3D materials and even compared to ultra-thin-body silicon, because, in the case of a 2D material, the field lines must pass through a vdW gap between the 2D layer and the dielectric/substrate, while no such gap exists for 3D materials. ^{18,19} This reduced screening in 2D materials causes a "renormalization" of dopant binding energies, typically resulting in dopant energy levels far from the band edges. ²⁰ Because of the combination of weak screening and the bandgap increase as the number of layers decrease in 2D materials [see Fig. 1(b)], dopant energy levels in monolayer TMDs can often be described as deep-levels, resulting in high ionization energies and low thermal activation rates of dopants. For example, in monolayer thick TMDs, even relatively shallow-level dopants have ionization energies ranging

between 100 and 200 meV, 21 and, consequently, under normal doping concentrations, minimal increase in conductivity is observed at room temperature. High impurity densities, sometimes in the alloying limits (> 5%), may be required to offset this high ionization energy of the dopants. Additionally, to address the issue of $R_{\rm C}$, very high doping-induced phase engineering or degenerate doping in the localized contact region is needed. At such high doping levels, one must be cognizant not only of the doping chemistry but also the effect of the dopants on the physical properties of the atomically thin film. Therefore, doping methods that can offer stable and scalable doping—up to the desired levels and in a nondestructive manner—are desired. In Secs. II–VIII, we discuss the advantages and the underlying limitations of a variety of traditional and emerging doping methods, which lead to our Perspective that substitutional doping is the best option for TMD-based transistors.

II. ELECTROSTATIC DOPING

One of the most popular doping methods in practice is based on electrostatic doping where the source/drain contact regions are gated (normally through a global back gate). Contrary to the traditional practice of using substitutional doping to degenerately dope the source/drain regions—using very high levels of boron or arsenic doping in silicon, for example—in electrostatic doping, a gate modulates the carrier density in the contact region and reduces the Schottky barrier (SB) width to enable efficient carrier injection into the channel region through tunneling. This impurity-free doping solution is non-destructive, and the conductivity is enhanced without changing the chemical composition or perturbing the crystal lattice of the 2D material. Figures 2(a) and 2(b) show a schematic of the commonly used device structure and the resulting band diagram across the metal/semiconductor junction.

This method is very commonly used in TMD transistors because the scientific community has not yet figured out how to achieve degenerate doping in TMDs analogous to those used in Si. Instead, researchers rely on a back gate to control the band bending in the contact regions to reduce the contact resistance. Moreover, this method is popular because of the relatively simple fabrication process needed to demonstrate the potential of prototype devices in a university's lab setting: scotch tape assisted transfer of an exfoliated flake on a pre-

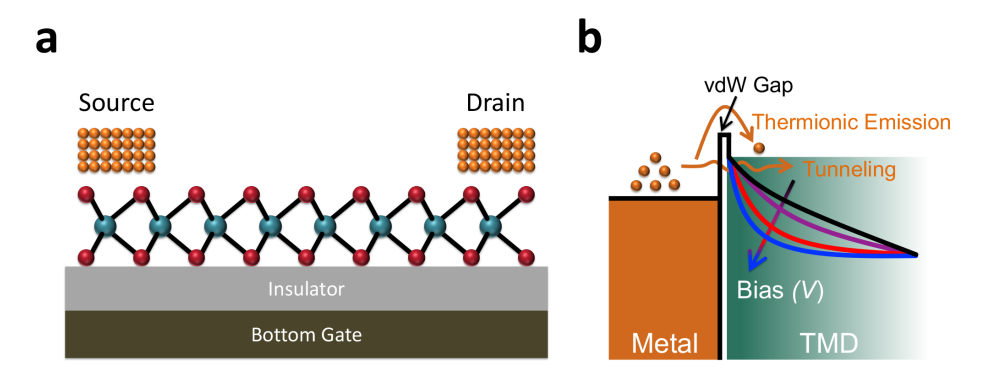


FIG. 2. (a) Schematic of a back-gated transistor with electrostatically gated contacts. The contact region is gated for efficient carrier injection in the channel region. Such a design increases the complexity and footprint of the circuit and results in significant RC delays. (b) Energy band diagram across the metal-vdW gap-TMD junction with thermionic emission and tunneling components highlighted. The voltage bias across the contact gate causes band-bending to favor more charge injection (electrons in this case) in the channel region through tunneling.

patterned SiO_2/Si substrate followed by a lithography step for source/drain electrode patterning makes it a very convenient method for quick electrical characterization. Although gated contact doping can be useful for demonstrating devices, it suffers from a variety of problems.

Device design for electrostatic doping requires an additional voltage source to gate the contacts compared to a heavily doped source/drain, which in turn increases the complexity of the circuitry and footprint of the overall chip. Moreover, high gate voltages are often required to induce stronger band-bending to achieve higher carrier densities (for higher $I_{\rm ON}$ and lower $R_{\rm C}$), which directly translates to more power consumption. In addition, the source/drain contact regions need to have significant overlap with the bottom gate, resulting in a high capacitive coupling and significant RC delays prohibiting ultra-fast switching operation. For all these reasons, we believe that focus should shift away from electrostatic doping to other more robust and scalable doping methods to enable the ultimate performance and scaling of TMD transistors.

III. SURFACE CHARGE TRANSFER DOPING

Instead of using an electric field, mono- or few-layers thick 2D films can be doped through the method of surface charge transfer doping, which relies on charge transfer between the 2D film and its

surroundings (e.g., surface adsorbates, adlayers/dielectric overlayers, substrate). 12 The exposed basal plane of 2D materials make it very convenient for the dopants to attach to the surface through a chemical bond or physisorption and dope it. As shown in Fig. 3(a), a difference in work function/energy-level/electronegativity between the dopant and semiconductor results in an injection or withdrawal of charge carriers from the 2D layer to modulate the electrical conductivity. Doping processes can be introduced under mild conditions and avoid any complexities such as ion-implantation or high-temperature diffusion. Dopants can also be deposited using solution processing methods such as spin-coating, drop-casting, or vapor-based methods, like evaporation. Such methods are convenient for mass production, are cost effective, and do not require any sophisticated setup. As shown in Fig. 3(b), one of the most prominent aspects of this doping method is that, unlike ion-implantation, it does not create disorder in the lattice of the TMD as the dopants lie out of the transport pathways and a high carrier mobility can be maintained in the channel region.

A variety of dopants and processes have been reported with each having its own merits and targeted toward specific applications. Decorating the TMD surface with metal nanoparticles, ^{22–24} chemical or plasma treatment, ^{25–28} and encapsulating the channel region with metal oxide/halide layers ^{29–33} are popular strategies (see Table I for a comparison of popular doping methods in the literature). Sarkar

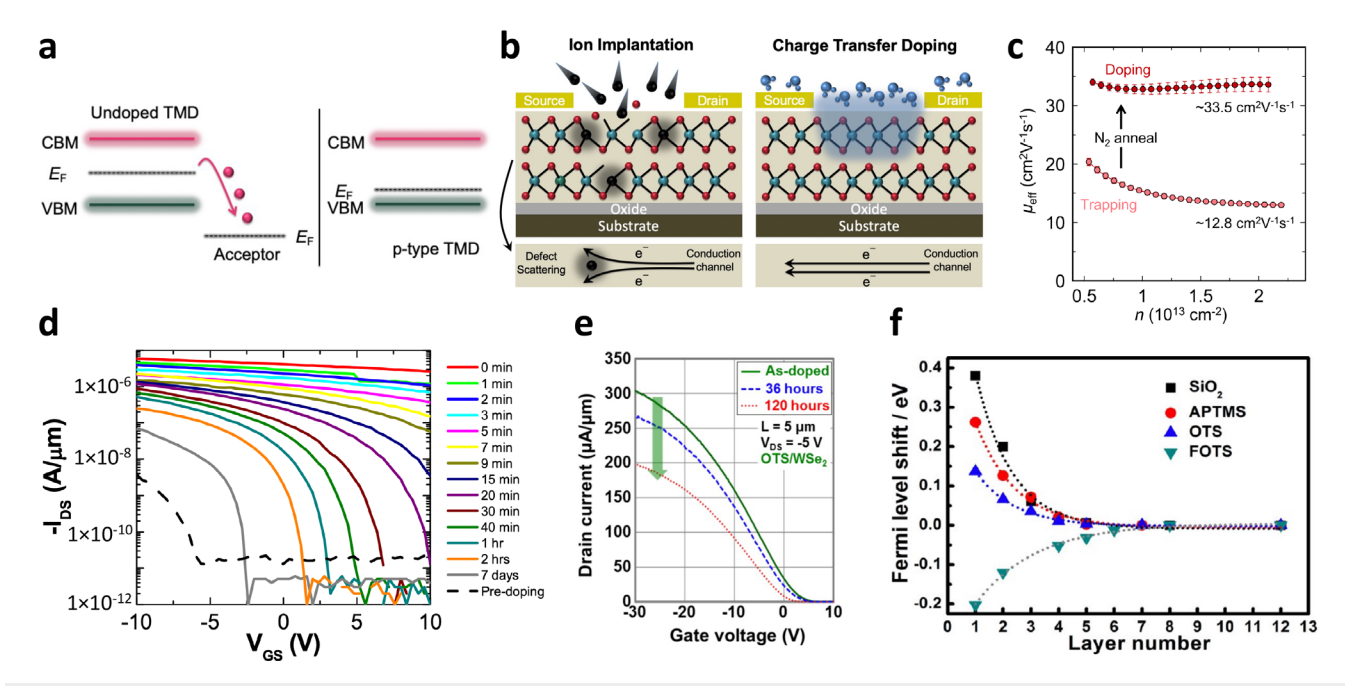


FIG. 3. (a) Acceptor type behavior of charge transfer doping in a semiconductor according to the Fermi level difference. (b) Schematic showing that where ion-implantation (on left) can result in creating defects in the crystal lattice to deteriorate the transport properties, charge transfer doping (on right) with its selective area doping and mild treatment does not create any disorder in the film. Because of this, impurity-induced scattering can be minimized and a high mobility can be maintained. Adapted with permission from Wang *et al.*, Nano Lett. **21**, 6298–6303 (2021). Copyright 2021 ACS. (c) Extracted $\mu_{\rm eff}$ showing 3× lower value for as-capped devices (large $\Delta D_{\rm il}$), but the $\mu_{\rm eff}$ recovers after the N₂ annealing. Reprinted with permission from McClellan *et al.*, Nano Lett. **15**, 1587–1596 (2021). Opyright 2021 ACS. (d) Transfer characteristics of a NO₂-doped WSe₂ FET, showing a gradual decrease in the doping effect over time due to the desorption of NO₂ molecules from the surface. Reprinted with permission from Fang *et al.*, Nano Lett. **12**, 3788–3792 (2012). Copyright 2012 ACS. (e) I_D –V_G curves of a SAM-doped WSe₂ photodetector. The on-current of the doped device was reduced by \sim 302 to \sim 199 $\mu N \mu m$) after 120 h of exposure in the air. Reprinted with permission from Kang *et al.*, Adv. Funct. Mater. **25**, 4219–4227 (2015). Copyright 2015 Wiley-VCH GmbH. (f) The Fermi level shift of MoS₂ nanoflakes on various substrates as a function of the number of layers. The doping effect is gradually suppressed as the thickness of the flake is increased. Reprinted with permission from Li *et al.*, ACS Nano. **7**, 7795–7804 (2013). Copyright 2013 ACS.

TABLE I. Comparison of popular doping techniques in the literature to reduce the contact resistance. ML refers to a monolayer. Superscripts denote how the carrier concentration was calculated in the referenced papers.

| Doping method | TMD | TMD thickness | Dopant | Doping type | Carrier concentration (cm ⁻²) | $R_{\rm C}$ (k $\Omega - \mu$ m) | Reference |
|-----------------|----------|------------------|-----------------------|----------------|---|----------------------------------|-----------|
| Charge transfer | MoS_2 | 1 ML | AlO_x | n-type | 2×10^{13a} | 0.48 | 34 |
| doping | MoS_2 | Few layer | K | n-type | 1×10^{13a} | | 89 |
| | MoS_2 | 5 nm | Benzyl Viologen (BV) | n-type | 1.2×10^{13a} | 1.1 | 90 |
| | WSe_2 | 1 ML | NO_2 | p-type | 2.2×10^{12a} | | 27 |
| | WSe_2 | Few layer | K | n-type | 2.5×10^{12a} | | 89 |
| | WSe_2 | 4 nm | MoO_3 | p-type | $\sim 5 \times 10^{13b}$ | 0.8 | 91 |
| | $MoSe_2$ | 1 ML | AlO_x | n-type | 5.5×10^{12b} | 1200 | 92 |
| | $MoSe_2$ | 2 ML | AlO_x | n-type | 1×10^{13b} | 60 | 92 |
| | $MoTe_2$ | 4.4 nm | O ₂ plasma | p-type | 2.5×10^{13a} | 0.6 | 93 |
| Intercalation | MoS_2 | 1-3 MLs | Li | n-type | $> 1 \times 10^{13a}$ | 0.2-0.3 | 49 |
| | WSe_2 | 2-5 MLs | Cs | n-type | ^c | 0.9 | 94 |
| | SnS_2 | 2 MLs | Cu | p-type | ^c | | 41 |
| Substitutional | MoS_2 | 1 ML | Re | n-type | 2.1×10^{12c} | | 83 |
| doping | MoS_2 | 1 ML | Nb | p-type | $4 \times 10^{14 \mathrm{d}}$ | | 95 |
| | MoS_2 | 1-2 nm | Cr | n-type | 3×10^{12b} | | 96 |
| | MoS_2 | | Nb | p-type | $1.8\times10^{14\rm d}$ | | 97 |
| | WSe_2 | 1 ML | Nb | p-type | 9×10^{11b} | 0.55 | 98 |
| | WSe_2 | 1 ML | V | p-type | 1.4×10^{12a} | | 1 |
| | $MoSe_2$ | 1 ML | W | p-type | 4×10^{11a} | | 99 |
| | WS_2 | 5-7 ML | Cl | n-type | 6×10^{11a} | 0.7 | 69 |
| | WS_2 | 4–8 nm | Cu | n-type | ^c | 7400 | 100 |

^aTransfer characteristics.

et al.²⁴ used the metal decoration method to study the effect of different metal work-functions on V_{th} shifts. Metals with high work functions (e.g., Pt) resulted in withdrawal of electrons from the TMD to induce p-type doping, while metals with lower work functions (e.g., Y) acted as n-type dopants. However, compared to the undoped devices, doped devices showed a significant degradation of the mobility. For example, WSe2 showed a degradation in mobility from 16.8 to 10.2 cm² (V s)⁻¹ after Pt deposition and higher doping led to a decrease in gate control and an increase in the subthreshold swing (SS). In a different approach, by taking advantage of the spatial selectivity of this doping method, Fang et al. 27 used nitric oxide (NO₂) chemical doping in the contact region of a monolayer WSe2 FET to create a highly doped junction with a steep profile, narrowing down the SB to enable efficient tunneling of holes for p-type doping. This resulted in $1000 \times$ improvement in I_{ON} and a near ideal SS of 60 mV dec⁻¹. Moreover, as the dopants were not lying in the transport pathway, an impressive hole mobility of 250 cm² (V s)⁻¹ was achieved in a monolayer FET. Later, Chiang et al., 28 used this NO_x treatment to dope the entire channel region of a monolayer WSe2 FET and showed record high hole current density of 300 μA/μm in WSe₂. McClellan et al.34 used metal oxide capping for doping, in which the capping layer offered an added advantage of protecting the device against degradation from air exposure. By using a sub-stoichiometric aluminum

oxide (AlO_x) layer on MoS₂, a record $I_{\rm ON}$ of 700 μ A/ μ m with $I_{\rm on}/I_{\rm off}$ ratio $> 10^6$ in a monolayer semiconductor was achieved. However, as shown in Fig. 3(c), the as-deposited AlO_x layer resulted in degradation of SS and mobility due to deep-level traps at the interface and required an additional step of N₂ annealing for recovery.

It is worth mentioning that not only the surface adsorbates but the substrate itself can also facilitate charge transfer. As reported by Zhang $et~al.,^{35}$ an approximately $10\times$ increase in mobility is observed for WSe2 films on h-BN compared to sapphire. Sapphire, being a relatively more reactive substrate, resulted in charge scattering, which degraded the mobility. h-BN with its inert surface and superior phonon spectra suppressed the effects of charged impurities and substrate phonons to help preserve the intrinsic properties of WSe2.

While all these results look very promising, there are some challenges as well. Fang $et\ al.$, showed that NO₂ (a dopant discussed above) has a high tendency to escape from the semiconductor's surface even at room temperature due to the weak physisorption of this gaseous dopant [Fig. 3(d)]. In another report on doping WSe₂ using a self-assembled monolayer (SAM), the doping effect was seen to gradually fade away over time due to the SAM reacting with moisture in the atmosphere [Fig. 3(e)]. Finally, as shown in Fig. 3(f), charge transfer doping worked on the outermost layer only, and the doping effect was found to be decreasing as the layer number increased.

 $^{^{}b}$ A parallel plate capacitor model (n = CV).

^cUnspecified/not applicable.

^dA Hall measurement.

IV. INTERCALATION DOPING

The ability of TMDs to serve as an intercalation host originates from their weak van der Waals forces, which allow a sufficient interlayer vdW gap that can accommodate the intercalation of foreign species. Atoms, ions, and even molecules can be intercalated to modulate the physical, electrical, and optical properties of TMDs. The method is particularly useful at inducing phase modulation, where a semiconductor TMD is converted to a semimetal or metal TMD, by incorporating a large amount of intercalated charge comparable to the initial semiconductor carrier concentration.

Intercalation can be achieved through a variety of ways including vapor phase, wet chemical, electrochemical, or solid phase methods. $^{43-45}$ A popular method is based on the diffusion of vaporized atoms into vdW gaps, where the composition can be varied by tuning the vapor pressures of the intercalants. 43 This intercalation is largely dependent on the size and electronegativity of the intercalant, with small size intercalants, such as alkali atoms, easier to intercalate due to their higher diffusivity. The modification in properties of the TMD host carries a wide range of effects, such as charge doping, hybridization, or lattice modulation. $^{46-48}$ In the case of charge transfer or hybridization, the Fermi level ($E_{\rm F}$) and the conductivity of the TMD is altered. In the case of lattice modulation, intercalation results in increasing the interlayer distance or changing the phase to modify the physical and electrical properties.

Phase engineering through intercalation can be very helpful to address the issue of contact resistance. By using a wet chemical method in which MoS₂ was soaked in a solution of n-butyllithium

(n-Bu-Li), Kappera *et al.*⁴⁹ showed that a metallic phase can be locally induced in an otherwise semiconducting phase of MoS₂-based transistors through lithium (Li) intercalation. Because of the carrier donation from the intercalant, the otherwise 2H lattice structure distorts to stabilize the electronic configuration by changing to the 1T phase. The undoped sample with 2H phase contacts had a $R_{\rm C}$ value of > 1 k Ω μ m, but the formation of a sharp 1T metal–2H semiconductor interface reduced $R_{\rm C}$ down to 200–300 Ω μ m at zero gate bias. In contrast to undoped devices having mobility values in the range of 15–20 cm² (V s)⁻¹, phase engineered contact FETs exhibited a mobility value of \sim 50 cm² (V s)⁻¹. This shows that, contrary to the contact gating used in electrostatic doping, if the contact region is highly doped, it does not need to be gated to achieve ultra-low $R_{\rm C}$ and high mobility.

In another report, Gong *et al.*⁴¹ used a solvent-based intercalation method to show p-type, n-type, and even degenerate doping in SnS_2 [Fig. 4(a)]. Where pristine SnS_2 showed typical n-type character because of the presence of sulfur vacancies, Cu intercalated bilayer SnS_2 showed a p-type conductivity with a hole field-effect mobility of \sim 40 cm² (V s)⁻¹. Intercalation with cobalt (Co), however, showed a metal-like behavior instead. Using lithography, selective area doping was used to make a variety of lateral heterostructures.

Another popular approach for intercalation doping employs an electrochemical cell with the intercalant working as an anode (e.g., Li), and the host TMD acting as a cathode are dipped in the liquid electrolyte to initiate the intercalation process. ⁵⁰ As the electrochemical reactions can be controlled by the magnitude and polarity of the applied voltage, this method enables controlled concentrations of the

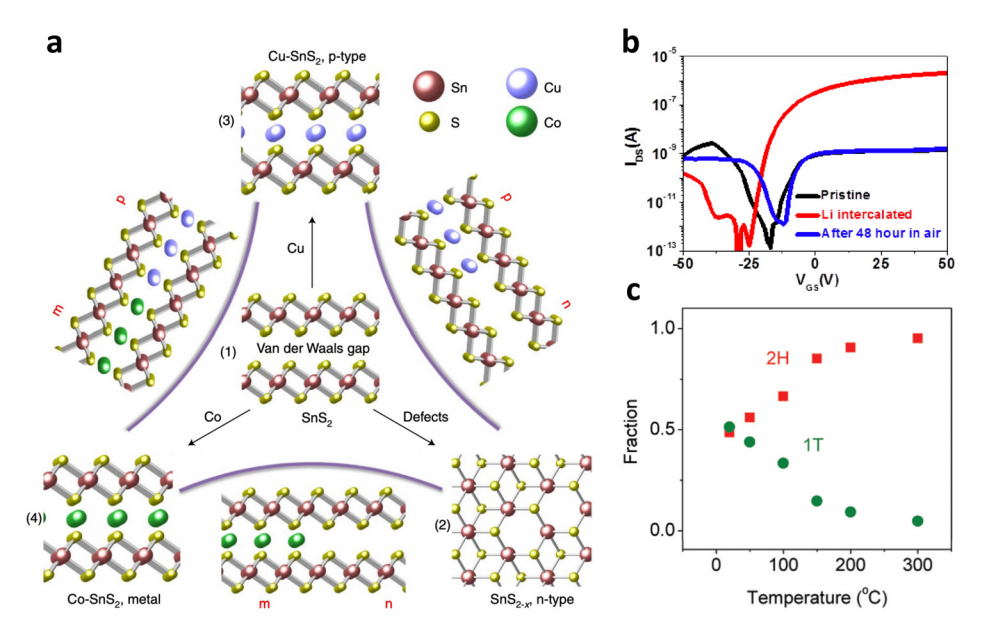


FIG. 4. (a) Schematics showing (1) pristine SnS₂, (2) n-type SnS₂ due to the presence of sulfur vacancies, (3) Cu-intercalated SnS₂ showing p-type conductivity, and (4) Co-intercalated SnS₂ as a highly conductive metal. Schematics between (2), (3), and (4) show that spatially controlled intercalation can help realize a variety of heterostructures. Reprinted with permission from Gong et al., Nat. Nanotechnol. 13, 294–299 (2018). Copyright 2018 Nature Publishing Group. (b) A comparison of transfer characteristics of a Li intercalated WSe₂ FET after keeping in air for 48 hrs. The ON current of the Li intercalated FET went back down to the levels of the undoped sample, while the OFF current is about 10 times higher. Reprinted with permission from Shin et al., Adv. Funct. Mater. 30, 2003688 (2020). Copyright 2020 Wiley-VCH GmbH. (c) XPS extracted relative fraction of 2H and 1T components of Li intercalated MoS₂. Degradation of the doping effect in MoS₂ as a function of annealing temperature is clear, because after a 300 °C annealing, the doped/phase transformed 1T metallic phase of MoS₂ is restored back to the original semiconducting 2H phase. Adapted with permission from Eda et al., Nano Lett. 11, 5111–5116 (2011). Copyright 2021 ACS.

intercalant and doping. Different from these solution-based or electrochemical methods, Liu *et al.*⁴⁴ used a solid-state method where a variety of homogenous Cu-intercalated TMD compounds were synthesized by mixing bulk Cu powder or foil with TMD powders. It was found that when Cu interacts with group IV or V TMDs, it can spontaneously transform into small size particles and can then self-intercalate in the vdW gap to yield ternary Cu_xMX_2 (0 < x \leq 1.2) compounds to impart n-type doping.

However, Shin *et al.*, ⁵¹ showed that the effect of Li intercalation in few layers thick WSe₂ transistors disappeared after exposure in air for 48 h [Fig. 4(b)]. This was attributed to the rapid oxidation of the highly reactive Li ions. In another report, Eda *et al.*⁵² showed that the intercalation doping effect started degrading at temperatures slightly above room temperature and was completely gone after a 300 °C annealing process [Fig. 4(c)], showing that this doping cannot survive even BEOL processing temperatures.

V. OTHER EMERGING DOPING METHODS

Apart from the doping methods just discussed, a variety of new doping methods have recently been reported in the literature and must be introduced to the reader to get a feel for where the community is searching. Lee et al. 13 first reported a doping strategy called "Reversible Solid-State Doping," which exploits a solid-state superionic phase transition material (silver iodide (AgI), for example) to induce switchable ionic doping in 2D materials. Contrary to ionic liquids/gels,⁵⁴ which offer nonvolatile doping only at cryogenic temperatures and are thus incompatible with mainstream solid-state electronics, the superionic AgI shows a sharp solid-state phase transition between insulating and conducting states to offer doping that is stable at above room temperature. As shown in Fig. 5(a), at a temperature higher than the superionic phase transition temperature (> 147 °C), an electric field was applied to the AgI microplates/WSe2 FETs through a back-gate with which Ag+ selectively accumulated or depleted at the WSe2 interface to impart n- or p-type character. A carrier-type switchable transistor was realized through reversible Ag+

migration by means of vertical poling where fully unipolar device behavior was observed in an otherwise ambipolar WSe₂ FET. A very notable aspect of this doping method is that the programmed functions can be erased by an external trigger such as temperature or UV irradiation.

In another report, Wang et al. 15 reported on a unique selfmodulated doping method called "Thickness Modulated Doping" in which, by varying the thickness of a 2D material (through mechanical exfoliation or Ar⁺ plasma thinning process), one can see a change in its doping type anywhere from p-type to intrinsic to n-type (up to degenerate levels). This doping strategy relies on the intrinsic defect concentration, where thickness-induced lattice deformation causes either metal or chalcogen vacancies, leading to a change in the conductance type of the film. As an example, the PtSSe system was studied where bulk films showed a high density of metal vacancies due to their low formation energy in thick films (confirmed by both DFT and STEM imaging) and were found responsible to cause p-type doping. On the other hand, relatively thin films showed a high density of chalcogen vacancies and, hence, n-type behavior. This was confirmed through a variety of electrical measurements, such as a shift in the threshold voltages as a function of layer thickness [see Fig. 5(b)]. Similar trends were reported in other TMDs including WSe₂, MoS₂, and MoTe2, where the thickness of the 2D film dictated the doping type.16

Another interesting new approach to TMD doping is "Remote Modulation Doping," introduced by Lee *et al.*, ¹⁴ to avoid ionized impurity scattering, which is intrinsic to substitutionally doped 2D films and causes mobility degradation. As shown in Fig. 5(c), by using a heterostructure—consisting of MoS₂ acting as an embedded channel material, hBN as a tunnel barrier, and a WSe₂ layer chemically doped with triphenylphosphine (PPh₃) to provide the doping effect—the carrier density in MoS₂ was modulated by remote charge transfer from the doped WSe₂ layer. As no ionized impurities or surface adsorbates were present in the carrier's pathway in the MoS₂ channel, high mobility was maintained. Temperature dependent mobility

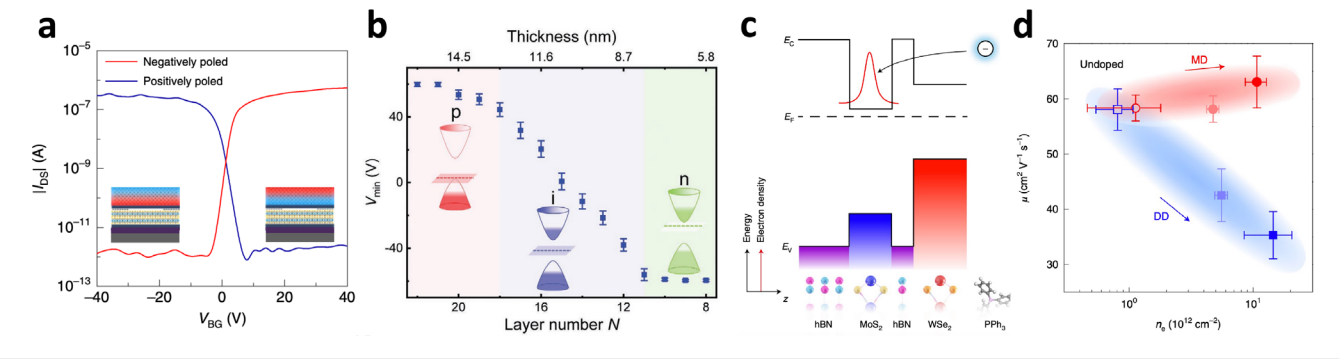


FIG. 5. (a) Transfer characteristics of a WSe₂ FET capped with silver iodide (AgI) after the vertical poling process with negative (red, $V_{BG} = -60 \text{ V}$) and positive (blue, $V_{BG} = +60 \text{ V}$) back gate voltages. Inset shows the schematics of the resulting ionic charge distribution. Reprinted with permission from Lee *et al.*, Nat. Electron 3, 630–637 (2020). Copyright 2020 Nature Publishing Group. (b) Minimum conductivity point (V_{min}) in the transfer characteristics of PtSSe FETs as a function of the layer thickness. V_{min} is the back-gate voltage value at which the drain-source current in the transfer characteristics is the minimum. Reprinted with permission from Wang *et al.*, Adv. Mater. 33, 2104942 (2021). Copyright 2021 Wiley-VCH GmbH. (c) Energy band diagram of the doped FET consisting of MoS₂ as the active channel material, hBN as the tunnel barrier WSe₂ as the chemically doped layer, and triphenylphosphine (PPh₃) as the n-type dopant. This structure results in confining the electrons in the conduction band of MoS₂. (d) Field-effect mobility (μ) as a function of the electron concentration (n_0) of the FETs before (open symbols) and after (filled symbols) doping. Squares represent the directly doped FETs, while circles represent the remote modulation-doped FETs. (c) and (d) reprinted with permission from Lee *et al.*, Nat. Electron 4, 664–670 (2021). Copyright 2021 Nature Publishing Group.

measurements were performed, which confirmed a significant suppression of impurity-induced scattering, since the electrons in the MoS_2 channel layer were spatially separated from the dopants (i.e., the doped WSe_2 layer). As shown in Fig. 5(d), remote modulation-doped MoS_2 FETs exhibited a room-temperature mobility of 60 cm^2 (V s) $^{-1}$, compared with a mobility of 35 cm^2 (V s) $^{-1}$ for directly doped devices. Moreover, where directly doped devices showed a drastic decrease in mobility as a function of carrier concentration (due to ionized impurity scattering), remote modulation-doped devices maintained their mobility for all carrier concentrations.

VI. CHALCOGEN SUBSTITUTIONAL DOPING

Extrinsic atoms can be incorporated directly into the lattice to permanently change its properties through substitution, a method that is at the core of silicon CMOS technology to control the

semiconductor's properties. As the process involves a chemical bond between the dopant and the host lattice, it is more stable and nonvolatile in comparison with the other methods discussed previously. Figures 6(a) and 6(b) show some of the commonly used substitutional dopants and how they sit inside the lattice.

In the X–M–X structure of TMDs, the chalcogens are exposed to the outer surface, which makes their substitution relatively easier. Doping during growth and post-growth both can be used to replace them. Interestingly, techniques that are normally used to grow high quality pristine TMDs may not be the ideal strategies for doping. For example, because of the low sticking coefficient of chalcogens, normally a chalcogen-rich growth environment is used to ensure vacancy free, stoichiometric films. Thewever, the presence of these same chalcogen vacancies can make substitution easier. Therefore, one smart strategy is to intentionally prepare chalcogen poor films or kick

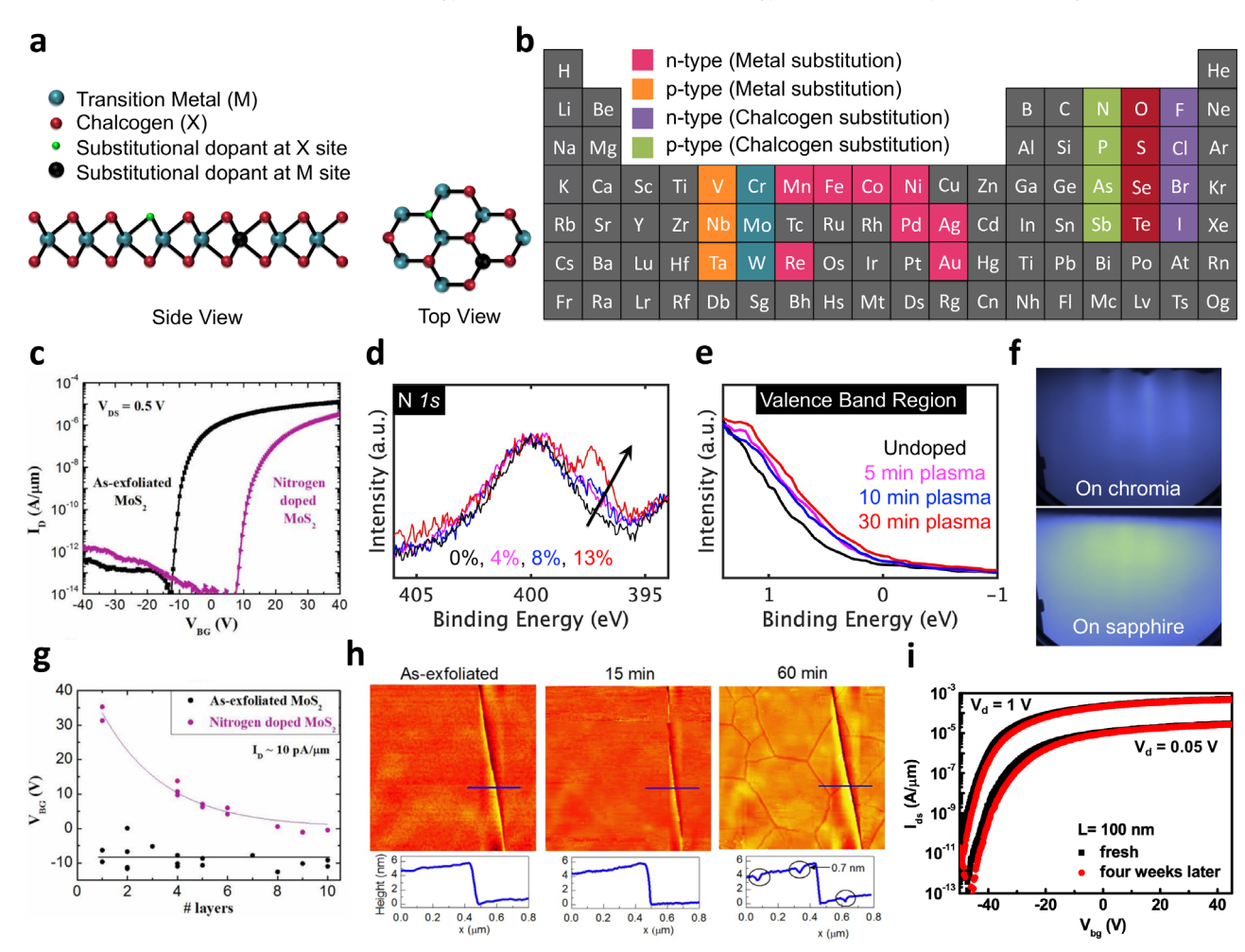


FIG. 6. (a) Schematic of a monolayer TMD with the substitutional dopants highlighted. (b) Common n- and p-type dopants for TMDs are highlighted. Adapted with permission from Loh *et al.*, Nano Res. **14**, 1668–1681 (2021). Copyright 2021 Tsinghua University Press and Springer-Verlag GmbH Germany, part of Springer Nature. (c) V_{th} shift confirming p-type doping effects. (d) XPS spectra of N 1s region of nitrogen-plasma-doped WSe₂ films. Up to 13% doping level was achieved. (e) Valence band maxima region showing p-type doping effect in nitrogen-doped WSe₂. (f) RHEED comparison of 30 min plasma-doped WSe₂ samples grown on chromia vs sapphire. (g) V_{th} as a function of the number of layers of MoS₂ showing that the doping effect gradually decreases as the number of layers increase. (h) AFM image showing surface damage after long time plasma exposure of MoS₂ flakes. (c), (g), and (h) reprinted with permission from Azcatl *et al.*, Nano Lett. **16**, 5437–5443 (2016). Copyright 2016 ACS. (i) Cl-doped MoS₂ FET, showing excellent stability over time. Reprinted with permission from Yang *et al.*, Nano Lett. **14**, 6275–6280 (2014). Copyright 2014 ACS.

out the chalcogens through some post growth process and then dope them. A very common method to do this is post-growth plasma treatment, which has the added advantage of excellent compatibility with CMOS processing. ^{58,59} High energy ions, generated through a radio frequency field are used to bombard the TMD surface to kick out and replace the chalcogens. Other techniques include thermal annealing, ⁶⁰ laser ablation, ⁶¹ or sputtering ⁶² to achieve the same goal. In addition to these, doping during growth—using molecular beam epitaxy (MBE) or metal organic chemical vapor deposition (MOCVD)—is also thermodynamically preferred in the presence of vacancies. ⁵⁷

A. p-type doping

Nitrogen and phosphorus act as p-type dopants for TMDs. A variety of methods such as post-growth plasma treatment,⁵ thermal annealing,⁶⁵ and direct growth techniques^{66,67} have been used and show promising chalcogen substitution for p-type effects. Azcatl et al. previously reported substitutional nitrogen doping in few layers thick exfoliated flakes of MoS₂ using a remote plasma technique.⁵⁹ The doping level was modulated by adjusting the gas flow, plasma power, and treatment time. Nitrogen substitution at chalcogen sites was confirmed in a variety of ways including an emergence of the N-Mo peak in x-ray photoelectron spectroscopy (XPS) and direct observation of nitrogen atoms sitting at sulfur sites in scanning transmission electron microscope (STEM) imaging. P-type doping was shown by a positive shift of the threshold voltage in the transfer characteristics [Fig. 6(c)] with a high hole doping level of 10^{19} cm⁻³. Later, we used MBE for in situ, post-growth doping of WSe2 where the doping level was controlled by changing the plasma exposure time, power, and pressure. As shown in Fig. 6(d), up to 13% doping was achieved in a bilayer of WSe2. P-type doping was confirmed by a gradual shift in the valence band maxima (VBM) toward the Fermi level as a function of doping [Fig. 6(e)]. Interestingly, it was found that the substrate plays a crucial role in the film quality and the resulting doping levels. Figure 6(f) shows a comparison of the reflection high energy electron diffraction (RHEED) pattern for a 30 min plasma-doped film grown on sapphire vs chromia. The RHEED pattern of the sample on sapphire is diffuse showing a degradation of the film quality post plasma doping, while a relatively better film quality was maintained on chromia (streaky RHEED). This is ascribed to a better lattice match between WSe2 and chromia where WSe2 grows epitaxially with a 30° rotation of the crystal lattice. This means that, contrary to the popular belief of epitaxy of the vdW materials, the lattice constant of the substrate does matter when it comes to growing/doping high quality 2D films. A prominent aspect of all these studies was that N-Metal bonds showed good thermal stability and survived even after 500 °C thermal annealing, which highlights the fact that these substitutionally doped TMDs can be used in nanoelectronic applications. As reported by Carvalho et al., 21 in 2D materials, the intrinsic carrier concentration is a relatively weak function of temperature as compared to 3D materials. As a result, the desired extrinsic doping regime is maintained to much higher temperatures in 2D semiconductors. 21 We believe that this very property, in conjunction with the fact that substitutional doping itself is thermally stable, makes TMD-based devices a possible route for high temperature environments and gives substitutional doping an obvious advantage over other doping methods such as intercalation or charge transfer doping that diminish with time at even moderate temperatures as described earlier.

Although post-growth patterned doping is one of the prerequisites for fabricating semiconductor devices, it has challenges of its own. As shown in Fig. 6(g), as in the case of charge transfer doping in MoS₂, post-growth plasma doping was restricted to the top few layers only, highlighting that further optimization is required to achieve uniform doping in thicker films. Also, as shown in Fig. 6(h), a long-time plasma exposure of MoS₂ flakes resulted in damage to the surface. In a related scenario, high-power plasma exposure caused chalcogen vacancies to induce n-type behavior and made p-type doping difficult. ⁶³ Therefore, there is a need to further investigate these post-growth treatments to come up with processes that offer uniform doping, up to the desired thickness of the film, without damaging it. An equal emphasis should be placed on *in situ* doping methods as well so that dopants can be introduced during the growth in a more uniform manner.

B. n-type doping

According to DFT calculations, chlorine (Cl), with an extra electron to donate, is a promising n-type dopant in TMDs. ⁶⁸ Yang et al., ⁶⁹ used Cl to dope few layers thick WS2 and MoS2 flakes and achieved a very high drain current of 380 μ A/ μ m. Exfoliated flakes were soaked in 1,2-dichloroethane (DCE), and chlorine substituted the chalcogens. A 2–3 orders of magnitude reduction in $R_{\rm C}$ was achieved through high electron doping ($\sim 10^{13} \, \mathrm{cm}^{-2}$), which resulted in a significant reduction in the Schottky barrier width allowing for efficient tunneling. In another study, a Cl-rich substrate was prepared by spin coating gold chloride hydrate as the chlorine source to prepare Cl-doped-MoS₂.⁷⁰ Where intercalated or charge transfer-doped devices start degrading after hours, these substitutionally doped devices showed excellent stability with minimal degradation even after four weeks [Fig. 6(i)]. Thus far, only Cl doping has been reported to induce n-type character through substitution at a chalcogen site. Some potential dopants could be other halogens that have shown promising n-type doping in II-VI materials, such as CdTe.7

This issue of limited reports on n-type doping in TMDs achieved exclusively through chalcogen substitution is multi-fold. As the native defects, such as chalcogen vacancies, are also believed to induce n-type character in TMDs (MoS₂ being a prime example), identification and decoupling the effect of just the dopants can be challenging. This issue is complex because the intrinsic defect density is corelated with the growth parameters and can also change in modified growth conditions. Furthermore, the interaction between the dopants and the vacancies can also impact the doping effects. ⁷³ Such issues highlight the need for indepth studies on dopants and their interaction with vacancies to enhance our understanding and, more importantly, to address the issue of $R_{\rm C}$ in n-type TMDs, which require high doping levels in the contact region.

VII. METAL SUBSTITUTIONAL DOPING

The metal atom can also be replaced through substitution in TMDs and, depending upon the valency of the dopant atom, one can get n- or p-type effects. Unlike dopants at the chalcogen sites, the overall stability of the dopants at metal sites in the lattice makes metal substituted TMDs potentially more desirable. This is because a dopant substituting a metal atom is secured by six covalent bonds (in the 1H phase), while a dopant replacing a chalcogen is only secured by three. As a result, metal substituted TMDs can retain these dopants and the

resulting doping effect more strongly. Furthermore, as highlighted in Fig. 6(b), a variety of metals can offer n-type doping, which, as discussed in Sec. VI, is harder to achieve through chalcogen substitution. Furthermore, by substituting magnetic impurities such as Fe, Co, or Mn in TMDs, one can change their magnetic properties, which is highly desirable for spin-based devices.

For metal substitution, a critical factor is the size of the dopant. If the size is sufficiently small, intercalation is preferred, while for larger atoms, substitution is favorable. It is important to highlight here that, because of the high stability of the transition metal in the lattice, along with the encapsulating chalcogenides acting as blocking layers, metal substitution through any post growth doping process is very difficult. As an example, where only 6–8 eV per atom is required to desorb a chalcogen atom, 20–30 eV per atom is required to desorb a transition metal atom. Therefore, doping during the growth is preferred for metal substitution, which works more efficiently when done in a metal-deficient or chalcogen-rich environment.

A. p-type doping

MoS₂, which is the most researched 2D material after graphene, shows n-type character in its pristine form due to the presence of sulfur vacancies, hydrogen interstitials, or H–S adatoms coming from the growth environment.^{76,77} However, to build complementary circuits using MoS₂ as the channel material, its p-type doping is also desired. Niobium (Nb) is one of the most researched p-type dopants to replace

Mo. Li et al.⁷⁸ used a one-step, salt-assisted CVD method to Nb-dope a monolayer of MoS₂. It was shown that upon doping, the naturally ntype conduction of MoS₂ was suppressed to a large degree, indicating that the doping has significantly compensated the heavily n-type character of MoS₂. Further annealing the devices in a sulfur atmosphere resulted in ambipolar characteristics due to the reduction of sulfur vacancies. Another p-type dopant is vanadium (V), which is predicted to produce dilute magnetic semiconductors in TMDs to potentially be used in spin-based electronics.⁷⁹ Here, we used MBE to grow V-doped monolayer WSe2 on a variety of substrates (e.g., sapphire, chromia, and GaN). Up to 30% V substitutional doping of W was achieved without encountering any phase separation. As shown in Fig. 7(a), high-angle annular dark field scanning transmission electron microscopy (HAADF-STEM) confirmed that the V atoms substitute the W atoms across the whole WSe2 flake in a uniform manner. Different from MBE, Yun et al. used CVD to synthesize V-WSe2 up to degenerate doping levels, which show that the substitutional doping is a very powerful method to tune the conductivity [Fig. 7(b)]. In another report, Chen et al., 80 used indium (In) to dope a monolayer of WS₂, another typically n-type TMD material. By using atmospheric pressure CVD, a controllable doping was realized by adjusting the weight ratio of the precursors.

Due to the aforementioned stability of the transition metal in the lattice, high temperature growths are required to substitute them. However, more scalable methods, especially BEOL compatible, are needed to bring M3D strategies into fruition. Here, Kozhakhmetov

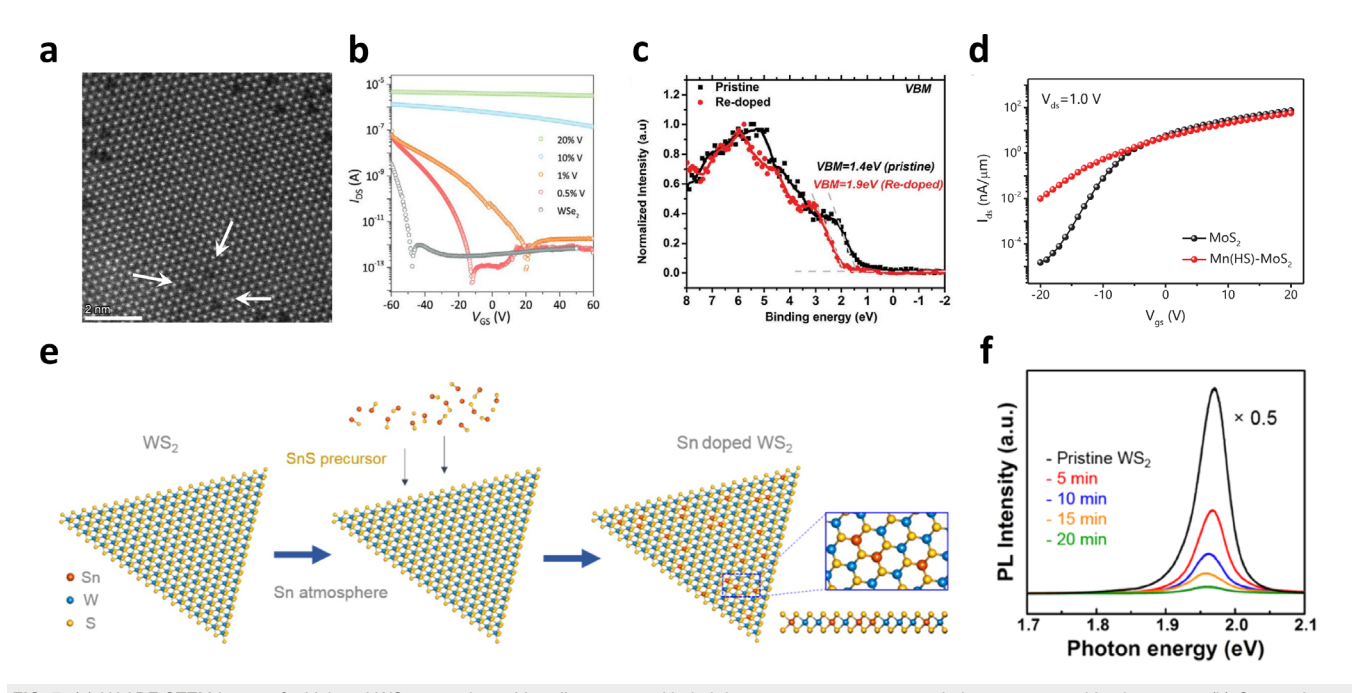


FIG. 7. (a) HAADF-STEM image of a V-doped WSe₂ monolayer. Vanadium atoms with their lower z-contrast appear as dark spots as noted by the arrows. (b) Output characteristics for V-doped WSe₂ FETs with various V-doping concentrations. Reprinted with permission from Yun *et al.*, Adv. Sci. 7, 1903076 (2020). Copyright 2020 Wiley-VCH GmbH. (c) Valence band maxima (VBM) comparison between undoped and Re-doped MoS₂. VBM after Re doping (plotted in red) moves further away from the Fermi level (located at 0 eV) indicative of n-type doping. Reprinted with permission from Zhang *et al.*, Adv. Funct. Mater. 28, 1706950 (2018). Copyright 2018 Wiley-VCH GmbH. (d) I–V curves of pristine and Mn-doped MoS₂ FETs. The negative shift of V_{th} and the lack of gate tunability suggest degenerate doping. I_{ON} did not improve. Reprinted with permission from Cai *et al.*, Small 16, 1903181 (2020). Copyright 2020 Wiley-VCH GmbH. (e) Schematic showing the formation of Sn-doped WS₂ monolayers. As-grown WS₂ monolayer is exposed to SnS precursor at a high temperature so that SnS can bind to the S vacancy sites for later metal (Sn) exchange. (f) PL spectrum of monolayer WS₂ before and after 5, 10, 15, and 20 min of Sn doping. (e) and (f) Reprinted with permission from Chang *et al.*, ACS Appl. Mater. Interfaces 11, 24279–24288 (2019). Copyright 2019 ACS.

et al.⁸¹ showed p-type V doping in WSe₂ at both FEOL and BEOL temperatures using MOCVD. WSe₂ FETs, which often exhibit ambipolar transport, were converted to unipolar, having a dominant hole branch.

From all such reports, it can be inferred that to achieve high metal substitution doping in TMDs, it is helpful if the dopant atoms form chalcogenides that are similar in structure to the chalcogenide that is being doped. For example, both NbS₂ and WS₂ share a similar trigonal prismatic (2H) structure and have very similar lattice constants. This ensures that upon substitution, no large strain is introduced and that the energy barrier for substitution is relatively small.

B. n-type doping

For group VI transition metals (Mo, W), group VII elements, such as rhenium (Re) and manganese (Mn), with an extra electron are potential n-type dopants. Gao *et al.*⁸² demonstrated *in situ* doping of Re (0.3%) in a monolayer of MoS₂ through a chemical vapor deposition method. Later, other groups extended the work to achieve even higher doping levels and showed nearly degenerate electron doping.⁸³ N-type doping was confirmed by a shift in the valence band maxima in XPS away from the Fermi level [Fig. 7(c)]. Interestingly, while the transfer characteristic showed a negative shift in $V_{\rm th}$ confirming n-type behavior, no improvement in the on-state current was seen. A similar situation was observed for the case of Mn doping as well [Fig. 7(d)],⁸⁴ where charged impurity scattering was suggested to be a possible reason for the mobility suppression. This is an area that needs to be studied further to identify doping solutions that can help improve electrical conductivity with minimal degradation of the mobility.

It is also important to highlight the versatility of substitutional dopants, as the same dopant can have a completely different effect in a different TMD. As reported by Kochat et~al., ⁸⁵ Re doping in MoSe₂ resulted in a phase transition from the semiconducting 2H phase to the metallic 1T phase. Such a metallic phase transition in the contact region can be used to achieve better R_c . Also interesting is the role of the substrate on some dopants. As reported by Zhang et~al., ⁸⁶ Mn was only incorporated in MoS₂ films when it was grown on an inert substrate like graphene. When the film was grown on a reactive substrate such as SiO₂, no Mn was incorporated. Photoluminescence (PL) of the doped samples was completely quenched causing loss of its optical properties as well. All the dopants were found to be reacting with the substrate, highlighting the fact that the substrate and TMD interaction can dominate the doping efficacy.

Finally, like in the case of the chalcogens, metals can also be substituted through post-growth doping processes. Chang *et al.*⁸⁷ demonstrated the postgrowth doping of tin (Sn) in WS₂ through a metal exchange mechanism, whereby Sn atoms substituted W to show n-type conductivity. As shown in Fig. 7(e), CVD grown films were exposed to a SnS precursor where a high temperature was used to create the S vacancies that acted as the initial binding sites for the SnS precursor for later metal (Sn) exchange. The PL spectra showed a gradual quenching with the increase in the treatment time, which was attributed to the increase in free electron concentration [see Fig. 7(f)]. However, like the case of chalcogen substitution in post-growth processes, doping was restricted to the top layer only, highlighting the need for optimized growth parameters to achieve a uniform doping through post-growth metal substitution.

VIII. CONCLUSION AND OUTLOOK

To continue advancement toward ultra-scaled, high-performance TMD-based transistors, scalable, consistent, and stable doping is of vital importance. Where doping levels in silicon-based FETs are usually on the order of 10^{17} – 10^{18} cm $^{-3}$, 2D materials require impurity concentrations in the percentage range to see noticeable improvement in electrical conductivity. This doping is needed to achieve higher $I_{\rm ON}$ and controlled threshold voltages and to address the issue of high contact resistance.

With so many methods actively being researched, a comparison has been provided to identify advantages and highlight the limitations of popular doping schemes. It is noted that despite being the easiest method to overcome high contact resistance and demonstrate working transistors, electrostatic doping will likely not be helpful in transitioning devices from lab to fab for a variety of reasons. As the device design for electrostatic doping requires an additional voltage source to gate the contacts, it increases the complexity of the circuitry and footprint of the overall chip. High gate voltages are often required to induce stronger band-bending to achieve higher carrier densities, which directly translates to more power consumption. Furthermore, as the source/drain contact regions need to have significant overlap with the bottom gate, it results in a high capacitive coupling/RC delay and prohibits ultra-fast switching operation.

The advantage of charge transfer doping is that it can be achieved at relatively low temperatures and is very effective to dope materials with high surface to volume ratio. However, our main criticism of this method is its poor stability and reliability. As discussed in Sec. III, the doping effect has been observed to degrade with time, even at room temperature, due to the weak physisorption of the dopants. Consequently, the doping process may not sustain the temperatures normally used in IC fabrication. Similarly, alkali metals, which are a very popular option for charge transfer doping, are so reactive that they easily oxidize in atmosphere and inevitably result in the degradation of device performance over time. ¹² Chemical treatment also raises instability concerns, as some chemical solutions are not very stable.³ Charge transfer doping is also very susceptible to the external environment, such as strain, electric field, or incident light, which further raises stability and reliability concerns.³⁸ Furthermore, dopants that can impart n-type character are generally not stable in the air due to their negative redox potential.3

Despite the availability of a variety of ways to induce intercalation and the doping levels that can be achieved, the stability and consistency in doping are major problems and make intercalation-doped TMD transistors unreliable. Another issue is the lack of available intercalant options to get both p- and n-type effects. Since the vdW gap of TMDs is sandwiched by negatively charged layers of anionic chalcogens, cation intercalation is feasible, but intercalation of anions is a big issue. ⁵³ While it may be too early to comment on the actual feasibility of other emerging doping methods (presented in Sec. V), we believe that each may have drawbacks for integrated circuits including high temperature instability and complicated device processing.

For robust, long-term doping, we firmly believe that substitutional doping is the most promising option due to its scalability, thermal stability, and rich choice of available dopants. The doping can be achieved using industry compatible methods such as plasma treatment, thermal diffusion, and *in situ* direct growth over a wide temperature window enabling both FEOL and BEOL integration. While we

acknowledge that there are issues with substitutional doping such as uniformity in post-growth doping, high ionization energy of the dopants, and dopant-induced mobility degradation, we believe that these challenges can be overcome and are not showstoppers that plague the other doping techniques. The potential advantage of this doping method clearly outweighs its limitations.

We would like to end by commenting that given the attention the community has endowed upon TMDs, the future of 2D materials for nanoelectronics looks promising. The field, which had started from studying a single material (graphene), has expanded to potentially hundreds of new materials, dopants, and their countless combinations. Indeed, there are challenges, but there are also an unimaginable number of opportunities.

ACKNOWLEDGMENTS

This work was supported in part by NEWLIMITS, a center in nCORE, a Semiconductor Research Corporation (SRC) program sponsored by NIST through Award No. 70NANB17H041. This work was also supported in part by the National Science Foundation (NSF) through the Division of Materials Research (DMR) Award No. 1921818. This work was supported in part by SUPREME, one of seven centers in JUMP 2.0, a Semiconductor Research Corporation (SRC) program sponsored by DARPA.

AUTHOR DECLARATIONS

Conflict of Interest

The authors have no conflicts to disclose.

Author Contributions

Rehan Younas: Conceptualization (supporting); Investigation (lead); Methodology (lead); Writing – original draft (lead). Guanyu Zhou: Conceptualization (supporting); Investigation (supporting); Methodology (supporting); Supervision (supporting); Writing – review & editing (supporting). Christopher L. Hinkle: Conceptualization (lead); Funding acquisition (lead); Supervision (lead); Validation (lead); Writing – review & editing (lead).

DATA AVAILABILITY

The data that support the findings of this study are available from the corresponding author upon reasonable request.

REFERENCES

- ¹S. J. Yun, D. L. Duong, D. M. Ha, K. Singh, T. L. Phan, W. Choi, Y. M. Kim, and Y. H. Lee, Adv. Sci. 7, 1903076 (2020).
- ²L. Rogée, L. Wang, Y. Zhang, S. Cai, P. Wang, M. Chhowalla, W. Ji, and S. P. Lau, Science **376**, 973 (2022).
- ³A. Chaves, J. G. Azadani, H. Alsalman, D. R. da Costa, R Frisenda, A. J. Chaves, S. H. Song, Y. D. Kim, D. He, J. Zhou, A. Castellanos-Gomez, F. M. Peeters, Z. Liu, C. L. Hinkle, S. H. Oh, P. D. Ye, S. J. Koester, Y. H. Lee, P. Avouris, X. Wang *et al.*, npj. 2D Mater. Appl. 4, 29 (2020).
- ⁴B. Radisavljevic, A. Radenovic, J. Brivio, V. Giacometti, and A. Kis, Nat. Nanotechnol. **6**, 147 (2011).
- ⁵Q. H. Wang, K. Kalantar-Zadeh, A. Kis, J. N. Coleman, and M. S. Strano, Nat. Nanotechnol. 7, 699 (2012).
- ⁶G. Zhou, T. Sun, R. Younas, and C. L. Hinkle, in *IEEE International Conference on Simulation of Semiconductor Processes and Devices, SISPAD* (IEEE, 2021), pp. 163–166.

- ⁷S. Das, A. Sebastian, E. Pop, C. J. McClellan, A. D. Franklin, T. Grasser, T. Knobloch, Y. Illarionov, A. v Penumatcha, J. Appenzeller, Z. Chen, W. Zhu, I. Asselberghs, L. J. Li, U. E. Avci, N. Bhat, T. D. Anthopoulos, and R. Singh, Nat. Electron. 4, 786 (2021).
- ⁸G. V. Resta, S. Sutar, Y. Balaji, D. Lin, P. Raghavan, I. Radu, F. Catthoor, A. Thean, P. E. Gaillardon, and G. de Micheli, Sci. Rep. 6, 29448 (2016).
- ⁹L. Loh, Z. Zhang, M. Bosman, and G. Eda, Nano Res. 14, 1668–1681 (2021).
- ¹⁰Y. Lv, W. Qin, C. Wang, L. Liao, and X. Liu, Adv. Electron. Mater. 5, 1800569 (2019).
- ¹¹Y. Jung, Y. Zhou, and J. J. Cha, Inorg. Chem. Front. **3**, 452 (2016).
- ¹²X. Zhang, Z. Shao, X. Zhang, Y. He, and J. Jie, Adv. Mater. 28, 10409 (2016).
- ¹³S. J. Lee, Z. Lin, J. Huang, C. S. Choi, P. Chen, Y. Liu, J. Guo, C. Jia, Y. Wang, L. Wang, Q. Liao, I. Shakir, X. Duan, B. Dunn, Y. Zhang, Y. Huang, and X. Duan, Nat. Electron. 3, 630 (2020).
- ¹⁴D. Lee, J. J. Lee, Y. S. Kim, Y. H. Kim, J. C. Kim, W. Huh, J. Lee, S. Park, H. Y. Jeong, Y. D. Kim, and C. H. Lee, Nat. Electron. 4, 664 (2021).
- ¹⁵Z. Wang, H. Xia, P. Wang, X. Zhou, C. Liu, Q. Zhang, F. Wang, M. Huang, S. Chen, P. Wu, Y. Chen, J Ye, S. Huang, H. Yan, L. Gu, J. Miao, T. Li, X. Chen, W. Lu, P. Zhou, and W. Hu, Adv. Mater. 33, 2104942 (2021).
- ¹⁶H. Xia, M. Luo, W. Wang, H. Wang, T. Li, Z. Wang, H. Xu, Y. Chen, Y. Zhou, F. Wang, R. Xie, P. Wang, W. Hu, and W. Lu, Light 11, 170 (2022).
- ¹⁷A. Chernikov, T. C. Berkelbach, H. M. Hill, A. Rigosi, Y. Li, O. B. Aslan, D. R. Reichman, M. S. Hybertsen, and T. F. Heinz, Phys. Rev. Lett. 113, 076802 (2014).
- ¹⁸M. Florian, M. Hartmann, A. Steinhoff, J. Klein, A. W. Holleitner, J. J. Finley, T. O. Wehling, M. Kaniber, and C. Gies, Nano Lett. 18, 2725 (2018).
- ¹⁹C. Gies and A. Steinhoff, Laser Photonics Rev. **15**, 2000482 (2021).
- ²⁰J. Hwang, C. Zhang, Y. S. Kim, R. M. Wallace, and K. Cho, Sci. Rep. 10, 4938 (2020).
- ²¹A. Carvalho and A. H. C. Neto, Phys. Rev. B **89**, 081406 (2014).
- ²²C. H. Chen, C. L. Wu, J. Pu, M. H. Chiu, P. Kumar, T. Takenobu, and L. J Li, 2D Mater. 1, 034001 (2014).
- ²³D. Qi, C. Han, X. Rong, X. W. Zhang, M. Chhowalla, A. T. S. Wee, and W. Zhang, ACS Nano 13, 9464 (2019).
- ²⁴D. Sarkar, X. Xie, J. Kang, H. Zhang, W. Liu, J. Navarrete, M. Moskovits, and K. Banerjee, Nano Lett. 15, 2852 (2015).
- ²⁵D. Qu, X. Liu, M. Huang, C. Lee, F. Ahmed, H. Kim, R. S. Ruoff, J. Hone, and W. J. Yoo, Adv. Mater. 29, 1606433 (2017).
- ²⁶Y. M. Chang, S. H. Yang, C. Y. Lin, C. H. Chen, C. H. Lien, W. B. Jian, K. Ueno, Y. W. Suen, K. Tsukagoshi, and Y. F. Lin, Adv. Mater. 30, 1706995 (2018)
- ²⁷H. Fang, S. Chuang, T. C. Chang, K. Takei, T. Takahashi, and A. Javey, Nano Lett. 12, 3788 (2012).
- ²⁸C. C. Chiang, H. Y. Lan, C. S. Pang, J. Appenzeller, and Z Chen, IEEE Electron Device Lett. 43, 319 (2022).
- ²⁹ A. Rai, A Valsaraj, H. C. P.Movva, A. Roy, R. Ghosh, S. Sonde, S. Kang, J. Chang, T. Trivedi, R. Dey, S. Guchhait, S. Larentis, L. F. Register, E. Tutuc, and S. K. Banerjee, Nano Lett. 15, 4329 (2015).
- ³⁰M. Yamamoto, S. Nakaharai, K. Ueno, and K. Tsukagoshi, Nano Lett. 16, 2720 (2016).
- ³¹T. D. Ngo, M. S. Choi, M. Lee, F. Ali, Y. Hassan, N. Ali, S. Liu, C. Lee, J. Hone, and W. J. Yo, Adv. Sci. 9, 2202465 (2022).
- ³²X. Liu, D. Qu, J. Ryu, F. Ahmed, Z. Yang, D. Lee, and W. J. Yoo, Adv. Mater. 28, 2345 (2016).
- ⁵³J. D. Lin, C. Han, F. Wang, R. Wang, D. Xiang, S. Qin, X. A. Zhang, L. Wang, H. Zhang, A. T. S. Wee, and W. Chen, ACS Nano 8, 5323 (2014).
- 34 C. J. McClellan, E. Yalon, K. K. H. Smithe, S. V. Suryavanshi, and E. Pop, ACS Nano 15, 1587 (2021).
- ³⁵X. Zhang, F. Zhang, Y. Wang, D. S. Schulman, T. Zhang, A. Bansal, N. Alem, S. Das, V. H. Crespi, M. Terrones, and J. M. Redwing, ACS Nano 13, 3341 (2019).
- ³⁶S. Li, Y. Ma, N. A. N. Ouedraogo, F. Liu, C. You, W. Deng, and Y. Zhang, Nano Res. 15, 123 (2022).
- ³⁷D. H. Kang, M. S. Kim, J. Shim, J. Jeon, H. Y. Park, W. S. Jung, H. Y. Yu, C. H. Pang, S. Lee, and J. H. Park, Adv. Funct. Mater. 25, 4219 (2015).
- 38 M. Muruganathan, J. Sun, T. Imamura, and H. Mizuta, Nano Lett. 15, 8176 (2015)

- ³⁹P. Luo, F. Zhuge, Q. Zhang, Y. Chen, L. Lv, Y. Huang, H. Li, and T. Zhai, Nanoscale Horiz. 4, 26 (2019).
- 40 Y. Li, C. Y. Xu, P. Hu, and L. Zhen, ACS Nano 7, 7795 (2013).
- ⁴¹Y. Gong, H. Yuan, C. L. Wu, P. Tang, S. Z. Yang, A. Yang, G. Li, B. Liu, J. van de Groep, M. L. Brongersma, M. F. Chisholm, S. C. Zhang, W. Zhou, and Y. Cui, Nat. Nanotechnol. 13, 294 (2018).
- ⁴²J. Wan, S. D. Lacey, J. Dai, W. Bao, M. S. Fuhrer, and L. Hu, Chem. Soc. Rev. 45, 6742 (2016).
- ⁴³S. J. R. Tan, I. Abdelwahab, Z. Ding, X. Zhao, T. Yang, G. Z. J. Loke, H. Lin, I. Verzhbitskiy, S. M. Poh, H. Xu, C. T. Nai, W. Zhou, G. Eda, B. Jia, and K. P. Loh, J. Am. Chem. Soc. 139, 2504 (2017).
- ⁴⁴X.-C. Liu, S. Zhao, X. Sun, L. Deng, X. Zou, Y. Hu, Y.-X. Wang, C.-W. Chu, J. Li, J. Wu, F.-S. Ke, and P. M. Ajayan, Sci. Adv. 6, eaay4092 (2020).
- ⁴⁵M. Wang, D. Williams, G. Lahti, S. Teshima, D. D. Aguilar, R. Perry, and K. J. Koski, 2D Mater. 5, 045005 (2018).
- ⁴⁶Q. Huang, X. Li, M. Sun, L. Zhang, C. Song, L. Zhu, P. Chen, Z. Xu, W. Wang, and X. Bai, Adv. Mater. Interfaces 4, 2108017 (2017).
- ⁴⁷X. Zhao, P. Song, C. Wang, A. C. Riis-Jensen, W. Fu, Y. Deng, D. Wan, L. Kang, S. Ning, J. Dan, T Venkatesan, Z. Liu, W. Zhou, K. S. Thygesen, X. Luo, S. J. Pennycook, and K. P. Loh, Nature 581, 171 (2020).
- ⁴⁸Z. Lin, Y. Liu, U. Halim, M. Ding, Y. Liu, Y. Wang, C. Jia, P. Chen, X. Duan, C. Wang, F. Song, M. Li, C. Wan, Y. Huang, and X. Duan, Nature **562**, 254 (2018).
- ⁴⁹R. Kappera, D. Voiry, S. E. Yalcin, B. Branch, G. Gupta, A. D. Mohite, and M. Chhowalla, Nat. Mater. 13, 1128 (2014).
- ⁵⁰Q. He, Z. Lin, M. Ding, A. Yin, U. Halim, C. Wang, Y. Liu, H. C. Cheng, Y. Huang, and X. Duan, Nano Lett. 19, 6819 (2019).
- ⁵¹Y. S. Shin, K. Lee, D. L. Duong, J. S. Kim, W. T. Kang, J. E. Kim, U. Y. Won, I. Lee, H. Lee, J. Heo, Y. H. Lee, and W. J. Yu, Adv. Funct. Mater. 30, 2003688 (2020).
- 52G. Eda, H. Yamaguchi, D. Voiry, T. Fujita, M. Chen, and M. Chhowalla, Nano Lett 11, 5111 (2011).
- 53 Z. Li, D. Li, H. Wang, P. Chen, L. Pi, X. Zhou, and T. Zhai, Small Methods 5, 2100567 (2021).
- ⁵⁴M. M. Perera, M. W. Lin, H. J. Chuang, B. P. Chamlagain, C. Wang, X. Tan, M. M. C. Cheng, D. Tománek, and Z. Zhou, ACS Nano 7, 4449 (2013).
- ⁵⁵R. Yue, Y. Nie, L. A. Walsh, R. Addou, C. Liang, N. Lu, A. T. Barton, H. Zhu, Z. Che, D. Barrera, L. Cheng, P. R. Cha, Y. J. Chabal, J. W. P. Hsu, J. Kim, M. J. Kim, L. Colombo, R. M. Wallace, K. Cho, and C. L. Hinkle, 2D Mater. 4, 045019 (2017).
- ⁵⁶H. P. Komsa and A. V. Krasheninnikov, *Phys. Rev. B* **91**, 125304 (2015).
- ⁵⁷K. Dolui, I. Rungger, C. das Pemmaraju, and S. Sanvito, Phys. Rev. B 88, 075420 (2013).
- ⁵⁸ A. Khosravi, R. Addou, C. M. Smyth, R. Yue, C. R. Cormier, J. Kim, C. L. Hinkle, and R. M. Wallace, APL Mater 6, 026603 (2018).
- ⁵⁹A. Azcatl, X. Qin, A. Prakash, C. Zhang, L. Cheng, Q. Wang, N. Lu, M. J. Kim, J. Kim, K. Cho, R Addou, C. L. Hinkle, J. Appenzeller, and R. M. Wallace, Nano Lett. 16, 5437 (2016).
- ⁶⁰H. Li, Q. Zhang, X. Duan, X. Wu, X. Fan, X. Zhu, X. Zhuang, W. Hu, H. Zhou, A. Pan, and X. Duan, J. Am. Chem. Soc. 137, 5284 (2015).
- ⁶¹E. Kim, C. Ko, K. Kim, Y. Chen, J. Suh, S. G. Ryu, K. Wu, X. Meng, A. Suslu, S. Tongay, J. Wu, and C. P. Grigoropoulos, Adv. Mater. 28, 341 (2016).
- ⁶²Q. Ma, M. Isarraraz, C. S. Wang, E. Preciado, V. Klee, S. Bobek, K. Yamaguchi, E. Li, P. M. Odenthal, A. Nguyen, D. Barroso, D. Sun, G. von Son Palacio, M. Gomez, A. Nguyen, D. Le, G. Pawin, J. Mann, T. F. Heinz, T. S. Rahman, and L. Bartels, ACS Nano 8, 4672 (2014).
- 63 Z. Jin, Z. Cai, X. Chen, and D. Wei, Nano Res. 11, 4923 (2018).
- ⁶⁴A. Nipane, D. Karmakar, N. Kaushik, S. Karande, and S. Lodha, ACS Nano 10, 2128 (2016).
- ⁶⁵Q. Yang, Z. Wang, L. Dong, W. Zhao, Y. Jin, L. Fang, B. Hu, and M. Dong, J. Phys. Chem. C 123, 10917 (2019).
- 66S. Qin, W. Lei, D. Liu, and Y. Chen, Sci. Rep. 4, 7582 (2014).
- ⁶⁷Q. Cao, Y. W. Dai, J. Xu, L. Chen, H. Zhu, Q. Q. Sun, and D. W. Zhang, ACS Appl. Mater. Interfaces 9, 18215 (2017).
- ⁶⁸J. Ma, Z. G. Yu, and Y. W. Zhang, Phys. Rev. B **95**, 165103 (2017).
- ⁶⁹L. Yang, K. Majumdar, H. Liu, Y. Du, H. Wu, M. Hatzistergos, P. Y. Hung, R. Tieckelmann, W. Tsai, C. Hobbs, and P. D. Ye, Nano Lett. 14, 6275 (2014).

- ⁷⁰S. Li, X. Chen, F. Liu, Y. Chen, B. Liu, W. Deng, B. An, F. Chu, G. Zhang, S. Li, X. Li, and Y. Zhang, ACS Appl. Mater. Interfaces 11, 11636 (2019).
- ⁷¹D. Rajavel and C. J. Summers, Appl. Phys. Lett. **60**, 2231 (1992).
- ⁷²A. Podestà, N. Armani, G. Salviati, N. Romeo, A. Bosio, and M. Prato, Thin Solid Films 511–512, 448 (2006).
- ⁷³S. J. Yun, B. W. Cho, T. Dinesh, D. H. Yang, Y. I. Kim, J. W. Jin, S. H. Yang, T. D. Nguyen, Y. M. Kim, K. K. Kim, D. L. Duong, S. G. Kim, and Y. H. Lee, Adv. Mater. 34, 2106551 (2022).
- 74Q. Yue, S. Chang, S. Qin, and J. Li, Phys. Lett. A 377, 1362 (2013).
- ⁷⁵Y. C. Lin, R. Torsi, D. B. Geohegan, J. A. Robinson, and K. Xiao, Adv. Sci. 8, 2004249 (2021).
- ⁷⁶A. Singh and A. K Singh, Phys. Rev. B **99**, 121201 (2019).
- 77 K. Dolui, I. Rungger, and S. Sanvito, Phys. Rev. B 87, 165402 (2013).
- ⁷⁸ M. Li, J. Yao, X. Wu, S. Zhang, B. Xing, X. Niu, X. Yan, Y. Yu, Y. Liu, and Y. Wang, ACS Appl. Mater. Interfaces 12, 6276 (2020).
- ⁷⁹S. Tiwari, M. L. van de Put, B. Sorée, and W. G. Vandenberghe, NPJ 2D Mater Appl. 5, 54 (2021).
- 80 Y. Chen, Y. Jiang, C. Yi, H. Liu, S. Chen, X. Sun, C. Ma, D. Li, C. He, Z. Luo, F. Jiang, W. Zheng, B. Zheng, B. Xu, Z. Xu, and A. Pan, Sci. China Mater. 64, 1449 (2021).
- 81 A. Kozhakhmetov, S. Stolz, A. M. Z. Tan, R. Pendurthi, S. Bachu, F. Turker, N. Alem, J. Kachian, S. Das, R. G. Hennig, O. Gröning, B. Schuler, and J. A. Robinson, Adv. Funct. Mater. 31, 2105252 (2021).
- 82 J. Gao, Y. D. Kim, L. Liang, J. C. Idrobo, P. Chow, J. Tan, B. Li, L. Li, B. G. Sumpter, T. M. Lu, V. Meunier, J. Hone, and N. Koratkar, Adv. Mater. 28, 9735 (2016).
- 83 K. Zhang, B. M. Bersch, J. Joshi, R. Addou, C. R. Cormier, C. Zhang, K. Xu, N. C. Briggs, K. Wang, S. Subramanian, K. Cho, S. Fullerton-Shirey, R. M. Wallace, P. M. Vora, and J. A. Robinson, Adv. Funct. Mater. 28, 1706950 (2018).
- ⁸⁴Z. Cai, T. Shen, Q. Zhu, S. Feng, Q. Yu, J. Liu, L. Tang, Y. Zhao, J. Wang, B. Liu, and H. M. Cheng, Small 16, 1903181 (2020).
- 85V. Kochat, A. Apte, J. A. Hachtel, H. Kumazoe, A. Krishnamoorthy, S. Susarla, J. C. Idrobo, F. Shimojo, P. Vashishta, R. Kalia, A. Nakano, C. S. Tiwary, and P. M. Ajayan, Adv. Mater. 29, 1703754 (2017).
- ⁸⁶ K. Zhang, S. Feng, J. Wang, A. Azcatl, N. Lu, R. Addou, N. Wang, C. Zhou, J. Lerach, V. Bojan, M. J. Kim, L. Q. Chen, R. M. Wallace, M. Terrones, J. Zhu, and J. A. Robinson, Nano Lett. 15, 6586 (2015).
- ⁸⁷R. J. Chang, Y. Sheng, G. H. Ryu, N. Mkhize, T. Chen, Y. Lu, J. Chen, J. K. Lee, H. Bhaskaran, and J. H. Warner, ACS Appl. Mater. Interfaces 11, 24279 (2019).
- 88D Wang, X. B. Li, and H. B Sun, Nano Lett. 21, 6298 (2021).
- ⁸⁹H. Fang, M. Tosun, G. Seol, T. C. Chang, K. Takei, J. Guo, and A. Javey, Nano Lett. 13, 1991 (2013).
- ⁹⁰D. Kiriya, M. Tosun, P. Zhao, J. S. Kang, and A. Javey, J. Am. Chem. Soc. 136, 7853 (2014).
- ⁹¹L. Cai, C. J. McClellan, A. L. Koh, H. Li, E. Yalon, E. Pop, and X. Zheng, Nano Lett. 17, 3854 (2017).
- ⁹²D. Somvanshi, E. Ber, C. S. Bailey, E. Pop, and E. Yalon, ACS Appl. Mater. Interfaces 12, 36355 (2020).
- 93X. Liu, D. Qu, Y. Yuan, J. Sun, and W. J. Yoo, ACS Appl. Mater. Interfaces 12, 26586 (2020)
- ⁹⁴Y. Zheng, D. Xiang, J. Zhang, R. Guo, W. Wang, T. Liu, L. Loh, Y. Wang, J. Gao, C. Han, M. Bosman, Z. Ni, and W. Chen, Nano Res. 14, 2703 (2021).
- ⁹⁵H. Gao, J. Suh, M. C. Cao, A. Y. Joe, F. Mujid, K. H. Lee, S. Xie, J. U. Lee, K. Kang, P. Kim, D. A. Muller, and J. Park, Nano Lett. 20, 4095 (2020).
- ⁹⁶C. Huang, Y. Jin, W. Wang, L. Tang, C. Song, and F. Xiu, J. Semicond. 38, 033004 (2017).
- ⁹⁷J. Suh, T. E. Park, D. Y. Lin, D. Fu, J. Park, H. J. Jung, Y. Chen, C. Ko, C. Jang, Y. Sun, R. Sinclair, J Chang, S. Tongay, and J. Wu, Nano Lett. 14, 6976 (2014).
- 98°S. K. Pandey, H. Alsalman, J. G. Azadani, N. Izquierdo, T. Low, and S. A. Campbell, Nanoscale 10, 21374 (2018).
- ⁹⁹ X. Li, M. W. Lin, L. Basile, S. M. Hus, A. A. Puretzky, J. Lee, Y. C. Kuo, L. Y. Chang, K. Wang, J. C. Idrobo, A. P. Li, C. H. Chen, C. M. Rouleau, D. B. Geohegan, and K. Xiao, Adv. Mater. 28, 8240 (2016).
- ¹⁰⁰M. Liu, S. Wei, S. Shahi, H. N. Jaiswal, P. Paletti, S. Fathipour, M. Remškar, J. Jiao, W. Hwang, F. Yao, and H. Li, Nanoscale 12, 17253 (2020).